The Astronomical Journal, 154:77 (8pp), 2017 August https://doi.org/10.3847/1538-3881/aa7fbc
© 2017. The American Astronomical Society. All rights reserved.

Detecting Proxima b's Atmosphere with *JWST* Targeting CO_2 at 15 μm Using a High-pass Spectral Filtering Technique

I. A. G. Snellen[1], J.-M. Désert[2], L. B. F. M. Waters[2,3], T. Robinson[4,13], V. Meadows[5], E. F. van Dishoeck[1], B. R. Brandl[1,6], T. Henning[7], J. Bouwman[7], F. Lahuis[3], M. Min[3], C. Lovis[8], C. Dominik[2], V. Van Eylen[1], D. Sing[9], G. Anglada-Escudé[10], J. L. Birkby[2,11], and M. Brogi[12,14]

[1] Leiden Observatory, Leiden University, Postbus 9513, 2300 RA Leiden, The Netherlands; snellen@strw.leidenuniv.nl
[2] Anton Pannekoek Institute for Astronomy, University of Amsterdam, P.O. Box 94249, 1090 GE Amsterdam, The Netherlands
[3] SRON Netherlands Institute for Space Research, Sorbonnelaan 2, 3584 CA Utrecht, The Netherlands
[4] Department of Astronomy and Astrophysics, University of California, Santa Cruz, CA 95064, USA
[5] Astronomy Department, University of Washington, USA
[6] Delft University of Technology, Faculty of Aerospace Engineering, Kluyverweg 1, 2629 HS Delft, The Netherlands
[7] Max-Planck-Institute for Astronomy, Koenigstuhl 17, D-69117 Heidelberg, Germany
[8] Observatoire de Genève, Université de Genève, 51 chemin des Maillettes, 1290 Versoix, Switzerland
[9] School of Physics, University of Exeter, Exeter, UK
[10] School of Physics and Astronomy, Queen Mary University of London, 327 Mile End Road, London E1 4NS, UK
[11] Harvard-Smithsonian Center for Astrophysics, 60 Garden Street, Cambridge MA 02138, USA
[12] Center for Astrophysics and Space Astronomy, University of Colorado at Boulder, Boulder, CO 80309, USA
Received 2017 May 3; revised 2017 July 6; accepted 2017 July 11; published 2017 August 1

Abstract

Exoplanet Proxima b will be an important laboratory for the search for extraterrestrial life for the decades ahead. Here, we discuss the prospects of detecting carbon dioxide at 15 μm using a spectral filtering technique with the Medium Resolution Spectrograph (MRS) mode of the Mid-Infrared Instrument (MIRI) on the James Webb Space Telescope (*JWST*). At superior conjunction, the planet is expected to show a contrast of up to 100 ppm with respect to the star. At a spectral resolving power of $R = 1790$–2640, about 100 spectral CO_2 features are visible within the 13.2–15.8 μm (3B) band, which can be combined to boost the planet atmospheric signal by a factor of 3–4, depending on the atmospheric temperature structure and CO_2 abundance. If atmospheric conditions are favorable (assuming an Earth-like atmosphere), with this new application to the cross-correlation technique, carbon dioxide can be detected within a few days of *JWST* observations. However, this can only be achieved if both the instrumental spectral response and the stellar spectrum can be determined to a relative precision of $\leqslant 1 \times 10^{-4}$ between adjacent spectral channels. Absolute flux calibration is not required, and the method is insensitive to the strong broadband variability of the host star. Precise calibration of the spectral features of the host star may only be attainable by obtaining deep observations of the system during inferior conjunction that serve as a reference. The high-pass filter spectroscopic technique with the MIRI MRS can be tested on warm Jupiters, Neptunes, and super-Earths with significantly higher planet/star contrast ratios than the Proxima system.

Key words: astrobiology – methods: data analysis – planetary systems – planets and satellites: atmospheres – planets and satellites: terrestrial planets

1. Introduction

The discovery of the exoplanet Proxima b through long-term radial velocity monitoring (Anglada-Escudé et al. 2016) is exciting for two reasons. First, it confirms that low-mass planets are very common around red dwarf stars, a picture that was already emerging from both transit and radial velocity surveys (Berta et al. 2013; Dressing & Charbonneau 2015). Second, the proximity of this likely temperate rocky planet at a mere 1.4 parsec from Earth makes it most favorable for atmospheric characterization, making Proxima b an important laboratory for the search for extraterrestrial life for the decades ahead.

Proxima b is found to orbit its host star in 11.2 days, placing it at an orbital distance of 0.0485 au. Since the luminosity of the host star is only 0.17% of that of our Sun, the level of stellar energy the planet receives is 30% less than the Earth, but nearly 70% more than Mars. This means that in principle it could have surface conditions that sustain liquid water—generally thought as a prerequisite for the emergence and evolution of biological activity (e.g., Kasting et al. 1993; Kopparapu et al. 2013). Although other habitats can be envisaged outside the so called "habitable zone" such as under the icy surface of Jupiter's moon Europa (e.g., Reynolds et al. 1983; Kargel et al. 2000), it is rather unlikely that signs of biological activity under such conditions could be detected in extrasolar planet systems (Lovelock 1965; Segura et al. 2005).

It is highly debatable whether Earth-mass planets in the habitable zones of red dwarf stars, such as Proxima b, could sustain or have ever sustained life. First, it is expected that the pre-main-sequence of red dwarf stars lasts up to a billion years during which the stellar luminosity is significantly higher than during the main-sequence lifetime of the star. This means that the planet will have had a significantly hotter climate early on, during which it may have lost most or maybe all of its potential water content (Ramirez & Kaltenegger 2014; Luger & Barnes 2015). Second, Proxima, as too are a large fraction of red dwarf stars, is a flare star that actively bombards the planet atmosphere with highly energetic photons and particles (Khodachenko et al. 2007; Lammer et al. 2007), possibly

[13] NASA Sagan Fellow.
[14] NASA Hubble Fellow.

causing a large fraction of the planet atmosphere to be lost. Third, planets in the habitable zone of red dwarf stars are expected to be tidally locked, and may be synchronously rotating—always faced with the same side to the host star (e.g., Barnes et al. 2016; Ribas et al. 2016). It is not clear whether a habitable climate can be sustained with such a configuration (e.g., Kite et al. 2011). However, several theoretical endeavours, also in the wake of the Proxima b discovery, show that despite these possible drawbacks, the planet may well host an atmosphere with liquid water on its surface (Tarter et al. 2007; Ribas et al. 2016; Turbet et al. 2016).

Several studies have investigated the potential detectability of Earth-like atmospheres of planets orbiting late M-dwarfs using high-dispersion spectroscopy. Snellen et al. (2013) calculated whether the transmission signature of molecular oxygen of a twin Earth-planet in front of a mid-M dwarf could be observed using high-dispersion spectroscopy (see also Rodler & López-Morales 2014) and showed that it would require a few dozen transits with the European Extremely Large Telescope (E-ELT) to reach a detection. However, it is very unlikely that Proxima b is transiting (Kipping et al. 2017). A more promising avenue is to combine high-dispersion spectroscopy with high-contrast imaging (HDS+HCI Sparks & Ford 2002; Riaud & Schneider 2007; Kawahara et al. 2014; Snellen et al. 2014, 2015; Luger et al. 2017). Snellen et al. (2015) simulated observations with the E-ELT using optical HDS+HCI of a then still hypothetical Earth-like planet around Proxima, showing that detection of such planet would be possible within one night. Recently, Lovis et al. (2016) argued that if the new ESPRESSO high-dispersion spectrograph at the ESO Very Large Telescope (VLT) can be coupled with the high-contrast imager SPHERE, and the latter has a major upgrade in adaptive optics and coronagraphic capabilities, a detection of Proxima b is within reach.

As the next generation of extremely large ground-based telescopes is at least 5–10 years away, the James Webb Space Telescope (*JWST*) could be a more immediate option to detect an atmospheric signature of Proxima b. Unfortunately, simple diffraction arguments tell us that the *JWST* is not large enough to spatially separate the planet from its host star—with a maximum elongation of 37 mas ($\sim 1\lambda/D$ at 1 μm). Several studies (Greene et al. 2016; de Wit et al. 2016) show that atmospheric characterization of super-Earths transiting small M-dwarf stars is within range of the *JWST*. However, the probability that Proxima b transits its host star is only 1.3%. Instead, Kreidberg & Loeb (2016) discuss the possibility of detecting the thermal phase curve with the *JWST* Mid-Infrared Instrument (MIRI), using its slitless 5–12 μm Low Resolution (LRS) mode. Because the planet is expected to be tidally locked, the night-to-dayside temperature gradient will result in a variation in apparent thermal flux as function of orbital phase. Depending on the orbital inclination, and on whether the planet has an atmosphere (which affects the redistribution of absorbed stellar energy around the planet), variations of up to $\sim$35 ppm are expected in the LRS wavelength regime. They show that in the ideal case of photon-limited precision, one can indeed detect the phase variation over a planet orbit (11.2 days–268 hr). However, a particular concern is the intrinsic variability of Proxima Cen—which is known to be a flare star. A month-long observation program of the *MOST* satellite (Davenport et al. 2016) detected on average two strong optical flares a day. Extrapolating their results to lower energies and mid-infrared wavelength implies that the star exhibits $\sim$50 flares a day at levels $>$500 ppm—an order of magnitude stronger than the expected phase variation amplitude of the planet. Hence, it will be challenging to discern the planet signal with such observations.

In this paper, we discuss a new application to the cross-correlation technique used to probe exoplanet atmospheres (e.g., Snellen et al. 2010), targeting the 15 μm CO_2 planet signal with the Medium Resolution Spectrograph (MRS) mode of MIRI. Importantly, it is unaffected by broadband flux variations of the host star. Furthermore, a detection of CO_2 would constitute conclusive evidence that Proxima b contains an atmosphere, and provide constraints to its temperature structure. If Proxima b is indeed a terrestrial planet that formed at or near its current semimajor axis, it would have been subjected to the super-luminous phase of the star for up to 160 My (Barnes et al. 2016). In this time, it may have undergone ocean loss and a runaway greenhouse, or had all but the heaviest molecules in its atmosphere stripped early on, with the possibility of longer-term replenishment by volcanic outgassing over its 5 Gyr history (Lammer et al. 2007; Meadows et al. 2016; Ribas et al. 2016). All of these evolutionary processes would have increased the likelihood that the planetary atmosphere currently contains CO_2. In Section 2, we describe the details of the method, of the MRS mode of MIRI, and present simulations, including atmospheric modeling. The results are presented and discussed in Section 3.

2. A High-pass Spectral Filtering Technique

The key to any exoplanet atmospheric observation is the ability to separate planet signatures from the overwhelming flux of the host star. The cross-correlation technique used to probe exoplanet atmospheres does not work in the case of Proxima b with the *JWST*, because the spectral resolution is not sufficient to use the change in the radial component of the planet orbital velocity to filter out the planet light (e.g., Snellen et al. 2010), neither is the angular resolution sufficient to separate the planet from the star (in which case the HDS+HCI technique could be used). In this case, we propose to use a new version of these techniques in which a spectral feature is targeted in the integrated planet+star spectrum that can be differentiated from the stellar spectrum and attributed to the planet. Generally, this would not work because it constitutes an absolute spectrophotometric measurement requiring instrumental calibration and knowledge of the stellar spectrum to a level significantly better than the planet signal. However, if the instrument spectral resolution is sufficiently high, the requirements on calibration and stellar spectrum knowledge can be significantly relaxed by probing the high-pass spectrally filtered signature instead of the absolute spectrophotometric signal. In this case, the planet signal is the difference in flux density relative to a low-resolution mean, e.g., in the case of a molecular band composed of a series of distinct absorption lines, the high-pass filtered spectral signature consists of series of peaks and valleys in the spectrum (Figure 1). This has the advantage that the planet signal is spread out over many pixels and consists of positive and negative high-frequency components. In particular, low-frequency components in the spectrum are notoriously difficult to calibrate due to required accuracies in the spectrum of the calibration source, and in stray-light and background corrections. However, these are not important in this case.

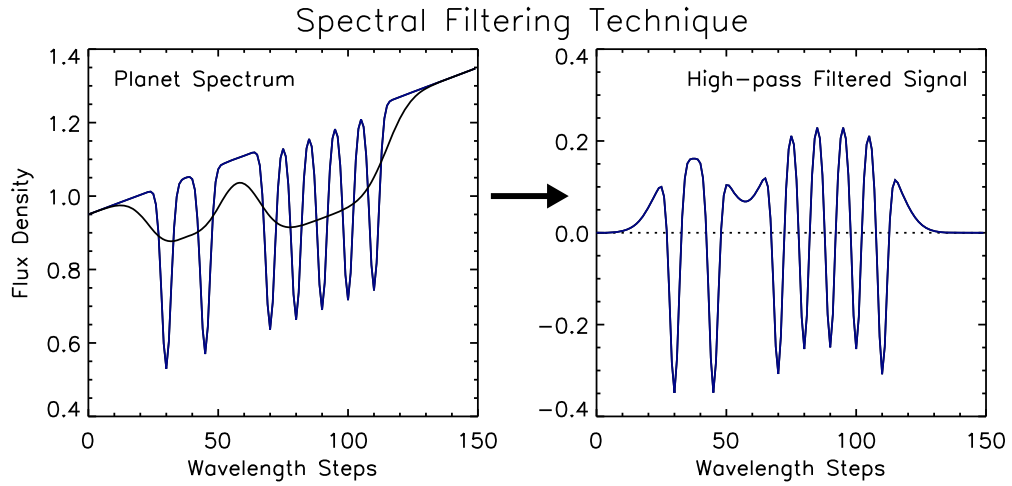

Figure 1. Schematic representation of the high-pass spectral technique. The left panel shows a toy-model planet spectrum (blue) with its low-resolution spectrum overlaid (black). The right panel shows the high-pass spectrally filtered signal consisting of the difference between the high- and low-resolution spectrum. Only the high-frequency components of the spectrum are preserved, making the high-pass filtered spectrum significantly easier to calibrate at a cost of information on the planet continuum flux level.

We argue that the spectral filtering technique will work well for the MRS mode of MIRI targeting CO_2 at 15 μm. In the case of Proxima b, its variations in the radial component of its orbital velocity of up to 50 km s^{-1} corresponds to a shift of ± 1 wavelength step, which may also be detected and subsequently constrain its orbital inclination.

2.1. MRS Mode of MIRI

The MRS mode of the MIRI (Rieke et al. 2015; Wright et al. 2015) on JWST utilizes an integral field spectrograph (IFS) that has four image slices producing dispersed images of the sky on two 1024 × 1024 infrared detector arrays, which provide $R =$ 1300–3600 integral field spectroscopy over a $\lambda = 5$–28.3 μm wavelength range (Wells et al. 2015; Labiano et al. 2016). The spectral window is divided into four channels covered by four integral field units: (1) 4.96–7.77 μm, (2) 7.71–11.90 μm, (3) 11.90–18.35 μm, and (4) 18.35–28.30 μm.

Two grating and dichroic wheels select the wavelength coverage within these four channels simultaneously, dividing each channel into three spectral sub-bands indicated by *A*, *B*, and *C*, respectively. To obtain a complete spectrum over the whole MIRI band, one has to combine exposures in the three spectral settings, *A*, *B*, and *C*. As we are primarily interested in the 15 μm CO_2 feature, only one setting will be sufficient: 3*B* covering the 13.2–15.8 μm range. Note that the same setting will deliver the 1*B* (5.6–6.7 μm), 2*B* (8.6–10.2 μm), and 4*B* (20.4–24.7 μm) wavelength ranges for free. Of these, 2*B* is particularly interesting because it contains the ozone absorption feature. This is briefly discussed in Section 3.5.

The IFS of Channel 3 consists of 16 slices (width = 0.″39), each containing 26 pixels (0.″24) providing a field of view of ∼6″ × 6″. The spectrum is dispersed over 1024 pixels (1 pix = 2.53 nm = 52 km s^{-1}) at a spectral resolving power of $R \sim$ 1790–2640 (168–113 km s^{-1}).

2.2. Modeling Proxima b and Its Atmosphere

Exoplanet Proxima b is found to orbit its host star in $11.186^{+0.001}_{-0.002}$ days (Anglada-Escudé et al. 2016). The amplitude of its radial velocity variations corresponds to a minimum mass of $1.27^{+0.19}_{-0.17}$ $M_{\rm Earth}$. If the mean density of the planet is the same as that of the Earth, and its orbit is nearly edge-on, it will have a radius of ∼1.1 $R_{\rm Earth}$. Proxima Cen has an estimated mass of 0.123 ± 0.006 $M_{\rm Sun}$, implying an orbital semimajor axis of $0.0485^{+0.0041}_{-0.0051}$ au, corresponding to a maximum angular separation of 37.5 mas. Proxima Cen has an effective temperature of $T_{\rm Eff} = 3042 \pm 117$ K, radius of 0.141 ± 0.007 $R_{\rm Sun}$, and bolometric luminosity of $L = 0.0017$ $L_{\rm Sun}$ (Doyle & Butler 1990; Ségransan et al. 2003; Demory et al. 2009).

Due to the close vicinity of the planet to its host star, it is generally assumed that Proxima b is tidally locked, meaning that the same dayside hemisphere is eternally facing the star. The planet effective dayside temperature will strongly depend on its Bond albedo and global circulation patterns. If, due to atmospheric circulation, the absorbed stellar energy is homogeneously distributed over the planet, and the Bond albedo is similar to that of Earth ($A_B = 0.306$), the dayside equilibrium temperature of Proxima b is 235 K. If there is effectively no circulation and the absorbed stellar energy is instantaneously reradiated, its observed dayside temperature could be as high as 300 K (and even up to 320 K for a moon-like albedo). In the other extreme case, in which the planet has an albedo comparable to Venus ($A_B = 0.9$) with a very effective atmospheric circulation, its dayside effective temperature could be as low as 145 K. For the calculations below, we assume a continuum brightness temperature of 280 K at 15 μm and a near-transiting orbital inclination, corresponding to a planet/star contrast ratio of 6×10^{-5} at superior conjunction.

Simulated high-resolution emission spectra of Proxima b were generated by the Spectral Mapping Atmospheric Radiative Transfer (SMART) model, assuming it to have an atmosphere such as Earth, using opacities from the Line-By-Line ABsorption Coefficient (LBLABC) tool (both developed by D. Crisp; see Meadows & Crisp 1996). The HITRAN 2012 line database (Rothman et al. 2013) was used as input to LBLABC, which generates opacities at ultra-fine resolution (resolving each line with >10 resolution elements within the half-width) on a grid of pressures and temperatures that spans a range relevant to Earth's atmosphere. Following this, SMART —which has been extensively validated against moderate- to high-resolution observations of Earth (Robinson et al. 2011)—

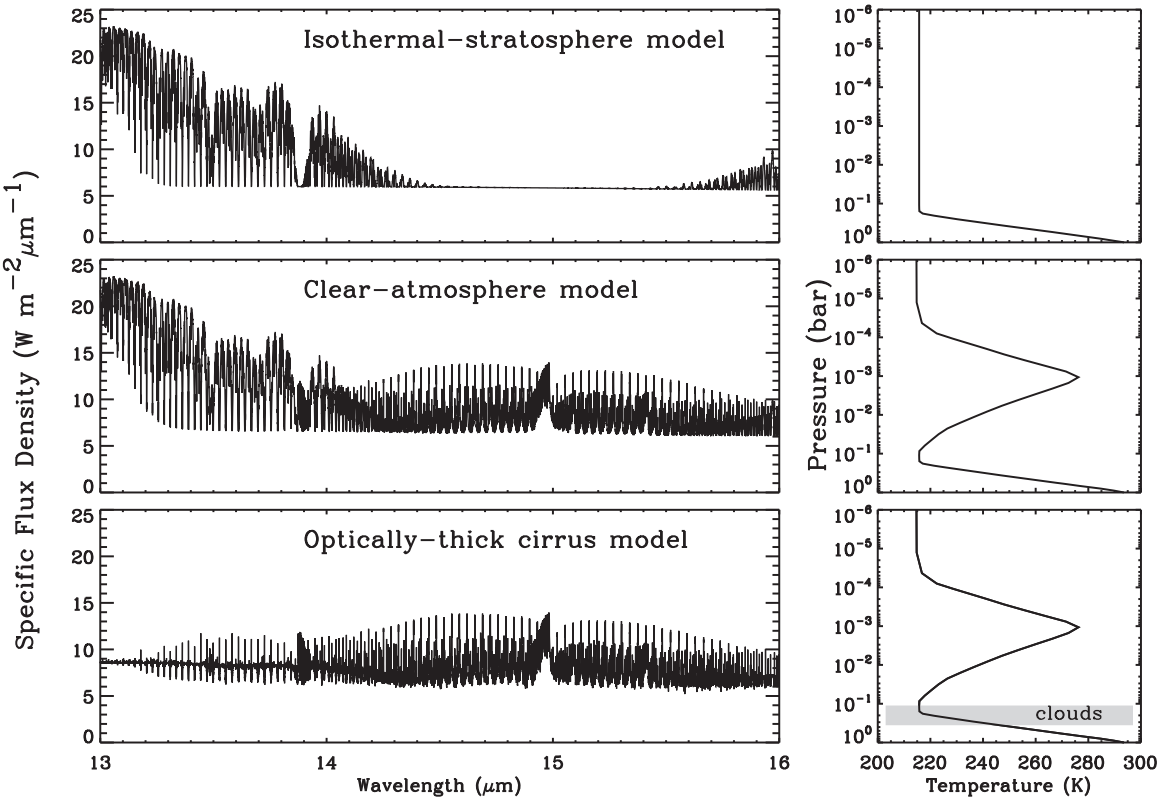

Figure 2. Planet model spectra (see Section 2.2) assuming a standard Earth atmospheric model for temperatures and gas mixing ratios, with, on the right, the assumed T/p profile. The upper panel shows the case where the stratospheric temperatures were artificially made isothermal and equal to the tropopause temperature (isothermal stratosphere model), the middle panel shows a model for clear sky conditions (clear atmosphere model), and the lower panel shows a spectrum for a case with opaque high-altitude cirrus clouds (optically thick cirrus model).

was used to simulate spectra at 5×10^{-3} cm^{-1} resolution (corresponding to $R > 10^5$ at the simulated wavelengths).

Our spectral simulations used a standard Earth atmospheric model for temperatures and gas mixing ratios (McClatchey et al. 1972), the spectra of which are shown in Figure 2. To bound certain extremes in thermal emission, model runs were performed for both clear sky conditions (the "clear atmosphere model") and for an opaque high-altitude cirrus cloud (located at 0.2 bar, near the tropopause Muinonen et al. 1989), called the "optically thick cirrus model". Also, to explore a situation with large thermal contrast between the surface and stratosphere, a case where Earth's stratospheric temperatures were artificially made isothermal and equal to the tropopause temperature (210 K) was simulated ("isothermal stratosphere model").

2.3. Simulated Observations

First, an estimate of the expected signal-to-noise ratio (S/N) for Proxima Cen with MIRI is obtained from the beta version of the *JWST* exposure time calculator.[15] The 12 μm and 22 μm flux densities of Proxima have been determined by the NASA *Wide-field Infrared Survey Explorer* (*WISE*) to be 924 mJy ($m_{W3} = 3.838 \pm 0.015$) and 278 mJy ($m_{W4} = 3.688 \pm 0.025$) respectively, which are fitted to a 3000 K Planck spectrum and subsequently interpolated to 13, 14, and 15 μm flux densities of 816, 713, and 630 mJy respectively. These fluxes are fed to the exposure time calculator for channel 3B of the MIRI MRS mode. A detector setup of 5 groups and fast readout gives an integration time of 16.6 s, delivering an S/N of 200 for a total exposure time of 38.85 s. This extrapolates to an S/N of 2000 hr^{-1} assuming that calibration uncertainties do not contribute to the noise.

The model planet spectra are smoothed to the spectral resolving power of $R = 2200$ (the mean of the MRS 3B band) and subsequently binned to the wavelength steps of the 3B MRS channel. The resulting clear-atmosphere model spectrum normalized by the stellar spectrum (which, for clarity, is assumed to be featureless) is shown in the top panel of Figure 3. Because the spectral filtering technique is only sensitive to the high-frequency signals, the low-frequency components are removed by subtracting a 25 wavelength-step sliding average (a rather arbitrary width) from the spectrum, resulting in the spectral differential spectrum shown in the middle panel. Subsequently, random noise is added to this differential spectrum at a level expected for the total simulated integration time, as shown in the bottom panel of Figure 3.

At this stage, it is determined at what statistical significance level the differential model spectrum is preferred to be present in the data with respect to pure noise. This is done by calculating the chi-squared (χ^2) of the observed spectrum, with its sliding average and differential model spectrum removed—for a range of planet/star contrasts and radial velocities. The minimum χ^2 is assigned as the best fit and the $\Delta\chi^2$ interval is used to determine the statistical uncertainties of a possible CO_2 detection. These simulations were repeated for the three different models, and for a range star/planet contrasts corresponding to different orbital phases or different effective dayside temperatures.

[15] http://jwst.etc.stsci.edu

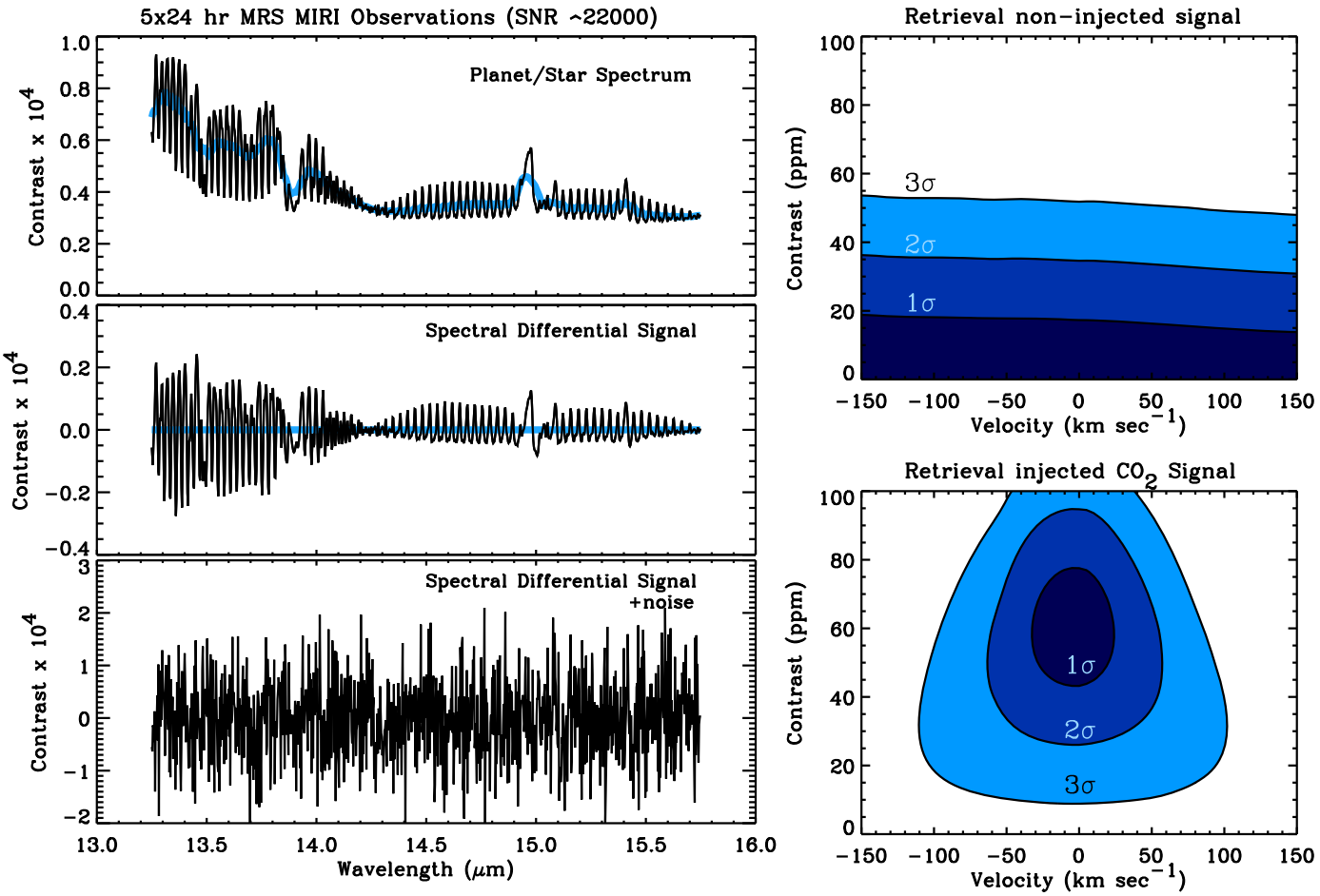

Figure 3. From model spectrum to simulated MRS MIRI observations assuming the clear-atmosphere model. The top-left panel shows the model spectrum convolved to the resolution of the MRS 3B channel of MIRI, normalized relative to the average star flux. The middle-left panel shows its associated high-pass spectral signal and the lower-left panel with noise added as if Proxima was observed for 5 × 24 hr. The top-right panel shows the statistical 1, 2, and 3σ confidence intervals when no CO_2 signal is present, pointing to a 3σ upper limit of 50 ppm for the planet/star contrast. The bottom-right panel shows the same, but with the simulated CO_2 signal present—detected at ~3.8σ. The *y*-axis indicates the mean planet/star contrast of the (non-spectrally filtered) template spectrum between 13.2 and 13.5 μm. Note that these simulations assume that both the instrumental spectral response and the stellar spectrum at a wavelength-to-wavelength scale have been determined, which is likely to require extra deep observations at inferior conjunction that serve as a reference (see Section 3.2).

3. Results and Discussion

3.1. Detectability

Our simulations show that the 15 μm CO_2 high-pass filtered signal of the Earth-mass planet can be detected within a limited amount of observing time. The MRS mode of MIRI at the *JWST* will, in 24 hr integration time (excluding overheads), deliver an $R = 1790$–2640 spectrum of Proxima Cen between 13.2 and 15.8 μm at a S/N of ~10,000 per wavelength step (assuming photon noise). This corresponds to a 1σ contrast limit of $\sim 1 \times 10^{-4}$. While the high-frequency features in the filtered planet spectrum are typically at a 1–3 $\times 10^{-5}$, there are about 100 within the targeted wavelength range—combining to a detection at a ~2σ level. It means that while the continuum planet/star contrast is at a level of 6×10^{-5} (~0.6σ per wavelength step), the combined spectrally filtered signal over the 3*B* band is about a factor of 3–4 higher. The top-right panel of Figure 3 shows the statistical confidence intervals for 5 × 24 hr of observations if no CO_2 signal is present, while the bottom-right panel shows the same, except with the clear-atmosphere CO_2 model spectrum for a face-on planet injected, indicating it can be detected at nearly 4σ within this exposure time. Hence, while the individual CO_2 features are not visible in the simulated spectrum, their combined signal can be clearly detected. Results are very similar for the Isothermal Stratosphere model and the Optically Thick Cirrus model.

3.2. Important Prerequisites

3.2.1. The Stellar Spectrum and Its Variability

We have made several assumptions that are vital for the high-pass spectral filtering technique to succeed in detecting CO_2 in Proxima b. First, it is assumed that the high-frequency components of the spectrum of the host star itself are perfectly known. Although low-resolution ($R = 600$) mid-infrared spectra of M-dwarfs taken with the *Spitzer Space Telescope* (Mainzer et al. 2007) seem featureless, Phoenix model spectra[16] (Allard et al. 2012) show that the 13.2–15.8 μm wavelength region of an M5V dwarf star harbours thousands of H_2O lines, collectively resulting in wavelength-to-wavelength variations of ~2% in the MIRI MRS spectrum. It means that these features need to be calibrated to better than a relative precision of 1% for them not to interfere with the planet CO_2

[16] https://phoenix.ens-lyon.fr/Grids/BT-Settl/CIFIST2011_2015/SPECTRA/

signal and not to act as an extra noise source. The star is also expected to have numerous but much weaker lines from hot CO_2 in this MRS band, resulting in wavelength-to-wavelength fluctuations of a few times 10^{-4}—hence, which need to be calibrated to a relative precision of ~10%. It is rather unlikely that spectral modeling could be sufficient to calibrate the high-frequency components of the mid-infrared spectrum to $\leqslant 10^{-4}$. This means that a deep stellar spectrum may need to be obtained near or at inferior conjunction when the contribution from planet emission from the system is the smallest, which would limit the sensitivity of this method for low orbital inclinations and would take as much time as the observations at superior conjunction.

As the data at superior and inferior conjunction must be taken at least ~5 days apart, variability of spectral features should also be below $\leqslant 10^{-4}$ on this timescale. We used archival data of Proxima from the UVES spectrograph ($R = 100{,}000$) at the VLT separated by 4 days (2009 October 10 and 14) to assess the optical variability of the star. For each of the two nights, a few dozen spectra were combined and the 868–878 nm wavelength range extracted, which is dominated by hundreds of TiO lines but is free of telluric lines. The averaged spectrum was subsequently convolved with a Gaussian to mimic the resolution of MIRI and subsequently binned to match its wavelength steps (in $\Delta\lambda/\lambda$). After dividing out a linear trend with wavelength, the standard deviation of the ratio of the resulting spectra of the two nights is 4×10^{-4}. Because these data are possibly limited by flat fielding uncertainties and variability in the mid-infrared is expected to be lower, this result is encouraging.

3.2.2. Instrument Calibration

Another prerequisite is that the spectral responses of the MRS pixels of MIRI can be adequately calibrated. Neither absolute flux calibration nor the low-frequency spectral response are important, but the sensitivity of one wavelength relative to the next is crucial—e.g., the spectral pixel-to-pixel calibration of the flat field. Potentially challenging is fringing, a common characteristic of infrared spectrometers. It is caused by interference at plane-parallel surfaces in the light-path of the instrument. Experiences with data from *ISO* and *Spitzer* show that it can be removed down to the noise level (e.g., Lahuis & van Dishoeck 2000). Wells et al. (2015) have characterized the fringing of the MIRI detectors in the laboratory and identify three fringe components with scale lengths (in wave number) of 2.8, 0.37, and 10–100 cm^{-1}, originating from the detector substrate, dichroic, and fringe beating, respectively. The planet CO_2 features also show a regular pattern, but with a characteristic scale length of ~1.6 cm^{-1}, which fortunately is significantly different from these fringe components. A potentially unwelcome source of error may be fringing in combination with dithering. Small residuals left over after defringing, combined from different dither positions, may be challenging to calibrate.

In the signal-to-noise calculations presented above, we assumed that the instrument calibration is perfect. For it not to add an extra source of noise, the wavelength-to-wavelength precision of the flat fielding and fringe removal must be $\leqslant 10^{-4}$. If this level can be reached for an individual IFS pixel, a tailored dithering strategy will subsequently push the calibration noise to below 10% of the noise budget for a 24 hr observation. A single observation will have the starlight mostly distributed over 2 slices × 2 pixels in the IFS, and by moving the star stepwise over the field of view of the IFS, about 80 independent positions can be obtained. This will reduce the calibration noise by a factor $\sqrt{2 \times 2 \times 80} \approx 15$.

3.2.3. Planet Spectrum

In addition, temporal stellar atmospheric disturbances can modify the chemical composition of a planet atmosphere, meaning that flares could temporarily change the CO_2 abundance of Proxima b. Such effects have been investigated by Venot et al. (2016), who find that although the abundances of some chemical species can be significantly altered deep into the atmosphere (~1 bar), CO_2 is expected to only be affected very high in the atmosphere at $<6 \times 10^{-4}$ mbar—suggesting that the 15 μm CO_2 will hardly be affected.

In principle, the observations could also be sensitive to other planets in the system. As such planets would likely be in a significantly wider orbit and be colder, the expected signal would be smaller. The CO_2 signals of such hypothetical planets could be distinguished from that of Proxima b, as their superior conjunctions would occur on different epochs.

3.3. Phase Variations

A detection of CO_2 will provide us with both the strength of the planet signal and its radial velocity. These can be used to constrain the orbital inclination of Proxima b. An example of such observation is shown in Figure 4, showing, in the left panel, the expected variation in contrast and radial velocity and their uncertainties for 9 × 24 hr exposures for each three measurements at orbital phase $\phi = 0.25$, 0.5, and 0.75—assuming an orbital inclination of near 90°. These represent significantly longer exposures than that presented in Figure 3. The right panel shows the same, but for an inclination of $i = 30°$, resulting in a smaller variation in contrast and radial velocity as a function of phase. The observations at inferior conjunction may need to serve as a reference for the stellar spectrum (see Section 3.2.1). In both cases, it is assumed that all thermal flux originated from the dayside hemisphere of the planet with an effective temperature of 280 K.

Because the strength of the signal at $\phi = 0.25$ and 0.75 can be up to a factor 2 lower than that at $\phi = 0.5$, calibration of the instrumental response and the stellar spectrum will be even more important. If the orbital inclination is low, the planet will never be seen entirely face-on, reducing the maximum signal at superior conjunction. However, it would also mean that the mass of the planet is higher, meaning that the planet radius could be larger than assumed above (in particular, if such more massive Proxima b is volatile rich), possibly counteracting the reduction in expected planet surface brightness.

3.4. Atmospheric Characterization

We performed our MRS MIRI simulations for three different atmospheric model spectra, (1) for a planet with an isothermal stratosphere, (2) for a planet with an inversion layer and clear atmosphere, and (3) with inversion layer combined with optically thick cirrus. Independent of which model we use, the increase in S/N over that expected for one wavelength step is very similar for all models, at a factor of 3–4. We also experimented by using the Earth transmission spectrum instead, which is similar to the isothermal stratosphere spectrum, but with a significant, differential signal at the heart of the CO_2

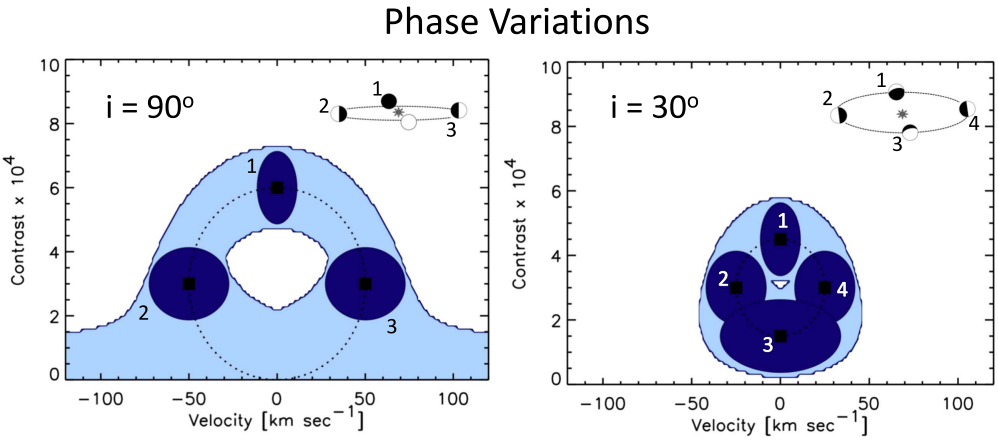

Figure 4. Examples of phase variation observations of the 15 μm CO_2 feature of Proxima b. The left shows the expected variation for an edge-on orbit, with the light blue regions indicating the 1σ confidence interval for a 9×24 hr observation at a given orbital phase (hence, nearly 650 hr of observations in total—significantly more than the simulations presented in Figure 3). The three dark-blue regions indicate the 1σ confidence intervals for particular observations at an orbital phase of $\phi = 0.5$ (superior conjunction), 0.25 and 0.75—showing the variation in radial velocity and contrast. The right panel shows the same but for an inclination of $i = 30°$, resulting in a smaller variation in contrast and radial velocity as function of phase. In both cases, it is assumed that all thermal flux originated from the dayside hemisphere of the planet with an effective temperature of 280 K.

band. This provides an S/N increase of a factor of ~5 over the S/N at at single wavelength step, which can be treated as an upper limit to the differential gain.

Retrieving an injected signal from one model using one of the other spectra results in a significant decrease in signal to noise—not surprising as a large number of the spectral features appear as either emission or absorption in the models. The brightness temperature of the planet atmosphere at a certain wavelength roughly corresponds to the atmospheric temperature at the $\tau = 1$ surface. In the center of the strongest CO_2 lines, where the opacity is greatest, we probe the atmosphere at the highest altitudes. Therefore, in the case of a strong thermal inversion (the clear-atmosphere and the optically thick cirrus models) the atmosphere will be warmer at such low pressure—resulting in emission lines instead of absorption lines when the atmosphere is cooler at higher altitudes. This implies that a detection will also constrain the temperature structure of the upper atmosphere, giving additional insights in high-altitude atmospheric processes. It will not just merely be a detection of the planet atmosphere, which can be compared with theoretical models. For example, Segura et al. (2005) argue that Earth-like planets orbiting M-dwarfs are likely to have relatively cool, bordering-on-isothermal stratospheres—even with O_3 present.

Several features from other molecules are present in the 13.2–15.8 μm wavelength range, such as C_2H_2 at 13.7 μm and HCN at 14 μm, which may be included in the atmospheric spectral template if needed (and if expected to be present in the planet atmosphere).

3.5. Prospects of Detecting Ozone

When CO_2 is targeted in the MRS 3*B* band, the 1*B*, 2*B*, and 4*B* bands are observed simultaneously. Interestingly, the 2*B* band, ranging from 8.6 to 10.3 μm covers the 9.6 μm ozone band. While CO_2 in the atmosphere of Proxima b may be likely, if the planet did undergo ocean loss early in its history to generate a massive O_2 atmosphere (Luger & Barnes 2015), it is also possible that O_3, photochemically produced from the O_2, is also present in higher abundances than is seen on Earth (Meadows et al. 2016). O_3 is of course also of high interest, as it can be used as a proxy for the O_2 biosignature from a photosynthetic biosphere. Detection of O_3 with *JWST* would therefore provide an intriguing first hint that life might be present on an extrasolar planet, although O_3 production via abiotic O_2 from ocean loss would first have to be ruled out.

The expected S/N per wavelength step in a 24 hr observation is 2×10^4, about a factor of 2 higher than in the 3*B* band because of the high stellar flux. On the other hand, the expected continuum planet/star contrast is a factor of ~2 lower compared to that expected at 15 μm. Unfortunately, the individual lines within the 9.6 μm band are more tightly packed than the lines in the 15 μm CO_2 band, i.e., the ozone band is not fully resolved at the MRS resolution of $R = 2800$ in this wavelength range. This means that if ozone is present in the atmosphere of Proxima b, its spectral differential signal will be about a factor of 3–4 smaller than that of CO_2. We estimate that in the best case one could expect a 2σ result in 20 days of *JWST* observing. We also note that the prerequisite for spectral calibration is also more stringent by a factor 2 compared to the CO_2 case. Hence, although observations of ozone come for free when the CO_2 band is targeted, it is unlikely this could result in a firm detection and is probably beyond the limit of what the *JWST* can achieve.

3.6. Strategy for Proof of Concept and Other Prospects

We envisage two ways to show proof of concept for the high-pass spectral filtering technique with the MRS mode of MIRI. First, the method can be used on exoplanet targets with significantly higher planet/star contrasts. For example, a $T = 1000$ K hot Jupiter orbiting a solar type star will have a 15 μm contrast of 10^{-3}, a factor 20 higher than Proxima b. It means that for a host star whose 15 μm flux is 40 times (4 magnitudes) fainter than Proxima b, CO_2 will still be detected 10× faster. Also, one could aim for cool Neptunes or super-Earths orbiting nearby M-dwarfs, such as Gliese 687b. If the spectrum of this particular planet exhibits a CO_2 absorption feature, it can be detected at a factor of 4 faster than in the case of Proxima b. From a theoretical point of view, it will be important to identify those planets that are expected to have CO_2 in their atmospheres and select those with the most favorable stellar magnitudes and planet/star contrasts.

Ultimately, one should target Proxima itself, gradually increasing the integration time and validating at each step that

the expected S/N limits are being reached. Detecting CO_2 in the atmosphere of Proxima b will be a major step forward in our quest for potential habitats and signs of extraterrestrial life.

The detection of specific spectral features expected in a planet atmosphere becomes orders of magnitude more powerful if the planet can also be angularly separated from the planet (e.g., Snellen et al. 2015). In such cases, the stellar spectrum can be effectively removed from all pixels in the IFU (as it is identical everywhere), after which the residual spectra can be searched for the planet features. H. J. Hoeijmakers et al. (2017, in preparation) show that this technique is very effective for the SINFONI and OSIRIS IFU spectrographs, located at the VLT and Keck Telescopes respectively, which have spectral resolving powers similar to that of MIRI (and the NIRSPEC IFU). If we could point the *JWST* directly at α Centauri A using the MIRI MRS, only 1″–1.″5 away the starlight is at the level of that of Proxima, implying that an Earth-sized planet in the habitable zone of α Cen A could possibly be detected in 24 hr. Unfortunately, α Centauri A will saturate the MIRI detectors within a small fraction of a second, irreversibly damaging the instrument. Possible ways to mitigate this issue need to be investigated.

I.A.G.S. acknowledges funding from the European Research Council (ERC) under the European Union's Horizon 2020 research and innovation programme under grant agreement No. 694513, and from research program VICI 639.043.107, which is financed by The Netherlands Organisation for Scientific Research (NWO). J.-M.D. acknowledges funding from the European Research Council (ERC) under the European Union's Horizon 2020 research and innovation programme (grant agreement nr 679633; Exo-Atmos). T.R. and J.L.B. gratefully acknowledge support from the National Aeronautics and Space Administration (NASA) through the Sagan Fellowship Program executed by the NASA Exoplanet Science Institute. Support for this work was provided in part by NASA through Hubble Fellowship grant *HST*-HF2-51336 awarded by the Space Telescope Science Institute, which is operated by the Association of Universities for Research in Astronomy, Inc., for NASA, under contract NAS5-26555. V.M. and T.R. are members of the NASA Astrobiology Institute's Virtual Planetary Laboratory Lead Team, supported by NASA under Cooperative Agreement No. NNA13AA93A.

ORCID

I. A. G. Snellen https://orcid.org/0000-0003-1624-3667
T. Robinson https://orcid.org/0000-0002-3196-414X
V. Meadows https://orcid.org/0000-0002-1386-1710
C. Dominik https://orcid.org/0000-0002-3393-2459
J. L. Birkby https://orcid.org/0000-0002-4125-0140
M. Brogi https://orcid.org/0000-0002-7704-0153

References

Allard, F., Homeier, D., & Freytag, B. 2012, RSPTA, 370, 2765
Anglada-Escudé, G., Amado, P. J., Barnes, J., et al. 2016, Natur, 536, 437
Barnes, R., Deitrick, R., Luger, R., et al. 2016, arXiv:1608.06919
Berta, Z. K., Irwin, J., & Charbonneau, D. 2013, ApJ, 775, 91
Davenport, J. R. A., Kipping, D. M., Sasselov, D., Matthews, J. M., & Cameron, C. 2016, ApJL, 829, L31
de Wit, J., Wakeford, H. R., Gillon, M., et al. 2016, Natur, 537, 69
Demory, B.-O., Ségransan, D., Forveille, T., et al. 2009, A&A, 505, 205
Doyle, J. G., & Butler, C. J. 1990, A&A, 235, 335
Dressing, C. D., & Charbonneau, D. 2015, ApJ, 807, 45
Greene, T. P., Line, M. R., Montero, C., et al. 2016, ApJ, 817, 17
Kargel, J. S., Kaye, J. Z., Head, J. W., et al. 2000, Icar, 148, 226
Kasting, J. F., Whitmire, D. P., & Reynolds, R. T. 1993, Icar, 101, 108
Kawahara, H., Murakami, N., Matsuo, T., & Kotani, T. 2014, ApJS, 212, 27
Khodachenko, M. L., Ribas, I., Lammer, H., et al. 2007, AsBio, 7, 167
Kipping, D. M., Cameron, C., Hartman, J. D., et al. 2017, AJ, 153, 93
Kite, E. S., Gaidos, E., & Manga, M. 2011, ApJ, 743, 41
Kopparapu, R. K., Ramirez, R., Kasting, J. F., et al. 2013, ApJ, 765, 131
Kreidberg, L., & Loeb, A. 2016, ApJL, 832, L12
Labiano, A., Azzollini, R., Bailey, J., et al. 2016, Proc. SPIE, 9910, 99102W
Lahuis, F., & van Dishoeck, E. F. 2000, A&A, 355, 699
Lammer, H., Lichtenegger, H. I. M., Kulikov, Y. N., et al. 2007, AsBio, 7, 185
Lovelock, J. E. 1965, Natur, 207, 568
Lovis, C., Snellen, I., Mouillet, D., et al. 2017, A&A, 599, A16
Luger, R., & Barnes, R. 2015, AsBio, 15, 119
Luger, R., Lustig-Yaeger, J., Fleming, D. P., et al. 2017, ApJ, 837, 63
Mainzer, A. K., Roellig, T. L., Saumon, D., et al. 2007, ApJ, 662, 1245
McClatchey, R. A., Fenn, R. W., Selby, J. E. A., Volz, F. E., & Garing, J. S. 1972, Optical Properties of the Atmosphere (3rd ed.; Bedford, MA: Air Force Cambridge Research Laboratories (OP))
Meadows, V. S., Arney, G. N., Schwieterman, E. W., et al. 2016, arXiv:1608.08620
Meadows, V. S., & Crisp, D. 1996, JGR, 101, 4595
Muinonen, K., Lumme, K., Peltoniemi, J., & Irvine, W. M. 1989, ApOpt, 28, 3051
Ramirez, R. M., & Kaltenegger, L. 2014, ApJL, 797, L25
Reynolds, R. T., Squyres, S. W., Colburn, D. S., & McKay, C. P. 1983, Icar, 56, 246
Riaud, P., & Schneider, J. 2007, A&A, 469, 355
Ribas, I., Bolmont, E., Selsis, F., et al. 2016, A&A, 596, A111
Rieke, G. H., Wright, G. S., Böker, T., et al. 2015, PASP, 127, 584
Robinson, T. D., Meadows, V. S., Crisp, D., et al. 2011, AsBio, 11, 393
Rodler, F., & López-Morales, M. 2014, ApJ, 781, 54
Rothman, L. S., Gordon, I. E., Babikov, Y., et al. 2013, JQSRT, 130, 4
Ségransan, D., Kervella, P., Forveille, T., & Queloz, D. 2003, A&A, 397, L5
Segura, A., Kasting, J. F., Meadows, V., et al. 2005, AsBio, 5, 706
Snellen, I., de Kok, R., Birkby, J. L., et al. 2015, A&A, 576, A59
Snellen, I. A. G., Brandl, B. R., de Kok, R. J., et al. 2014, Natur, 509, 63
Snellen, I. A. G., de Kok, R. J., de Mooij, E. J. W., & Albrecht, S. 2010, Natur, 465, 1049
Snellen, I. A. G., de Kok, R. J., le Poole, R., Brogi, M., & Birkby, J. 2013, ApJ, 764, 182
Sparks, W. B., & Ford, H. C. 2002, ApJ, 578, 543
Tarter, J. C., Backus, P. R., Mancinelli, R. L., et al. 2007, AsBio, 7, 30
Turbet, M., Leconte, J., Selsis, F., et al. 2016, A&A, 596, A112
Venot, O., Rocchetto, M., Carl, S., Roshni Hashim, A., & Decin, L. 2016, ApJ, 830, 77
Wells, M., Pel, J.-W., Glasse, A., et al. 2015, PASP, 127, 646
Wright, G. S., Wright, D., Goodson, G. B., et al. 2015, PASP, 127, 595